5066 *Chem. Mater.* **2009,** *21,* 5066–5071
DOI:10.1021/cm901369u

CHEMISTRY OF MATERIALS
Article

Novel Mn_3O_4 Micro-octahedra: Promising Cataluminescence Sensing Material for Acetone

Lichun Zhang,[†] Qin Zhou,[†] Zonghuai Liu,[‡] Xiandeng Hou,[†,§] Yubao Li,[§] and Yi Lv*,[†]

[†]*Key Laboratory of Green Chemistry & Technology, Ministry of Education, College of Chemistry, Sichuan University, Chengdu, Sichuan 610064, China,* [‡]*Key Laboratory of Applied Surface and Colloid Chemistry, Ministry of Education, School of Chemistry and Materials Science, Shaanxi Normal University, Xi'an 710062, China, and* [§]*Analytical & Testing Center, Sichuan University, Chengdu, Sichuan 610064, China*

Received May 19, 2009. Revised Manuscript Received September 15, 2009

Two novel morphologies of Mn_3O_4 micro-octahedra and hexagonal nanoplates were controllably synthesized by hydrothermal treatment of $KMnO_4$ in the dodecylamine-Na_2SO_3-ethanol/dodecylamine-ethanol system. XRD, SEM, HRTEM and N_2 adsorption measurements were used to characterize the prepared manganese oxide materials. With Mn_3O_4 micro-octahedra and hexagonal nanoplates as sensing materials, new acetone gas sensors were designed and their cataluminescence (CTL) property was evaluated. The effects of influencing parameters on the synthesis and sensing were studied. Experimental results show that the CTL properties of the prepared Mn_3O_4 materials are shape-dependent and Mn_3O_4 micro-octahedra show excellent sensing characteristics for acetone. Under the optimal experimental conditions, the calibration curve of the CTL intensity versus acetone vapor concentration was linear in ranges of 2.6−52.2 and 52.2−394.0 $\mu g\ mL^{-1}$, respectively, with a detection limit of 0.4 $\mu g\ mL^{-1}$ (signal/noise = 3) and a relative standard deviation in the range of 1 to 3%. For long-term stability, the signal variation for acetone concentration at 47 $\mu g\ mL^{-1}$ varied within ±11% in 6 months. The present sensor has a fast response time of 3 s and recovery time of less than 40 s.

Introduction

As the interest in the synthesis of micro/nano materials with tailored geometries has been sustainingly growing in recent years for their particular physical and chemical properties, more and more researchers have also paid their attention to the subsequent applications of micro/nano materials. Micro/nano materials are expected to play an important role in miniaturizing relevant devices because they can function as building blocks, especially in fabricating various sensors and the next generation of microelectronic/optoelectronic devices.[1−4] In recent years, cataluminescence (CTL) generated on the surface of nanomaterials has also been investigated as a promising transduction principle for gas sensors. In contrast to sensing based on intrinsic analyte properties, CTL approach dramatically expands the range of detectable species by utilizing a series of responsive sensing nanomaterials, improves sensors performance, and is adaptable for miniaturization.[5] Both Nakagawa[6] and Zhang[7] have poured much endeavor on the CTL studies and established a series of gas sensors by use of different catalytic nanomaterials, such as γ-Al_2O_3, TiO_2, and Fe_2O_3 nanotube. More recently, Zhang's group[8] assembled a catalytic optical chemo-sensor array for the CTL discrimination of ethanol, hydrogen sulfide, and trimethylamine in solution and a CTL-based imaging array for evaluation of the catalytic activities of different gold-supported catalysts. Yang et al.[9] have also developed a zeolite catalyst for the selective CTL detection of n-hexane. However, because of the multidimensional nature of the interactions between the function and the composition, preparation method, and end-use conditions of sensing materials, the exploration on sensing materials with new capacities is still a challenge.[5]

As an important functional metal oxide, manganese oxide (MnO_x) and its derivative compounds have attracted considerable attention in both academia and

*Corresponding author. E-mail: lvy@scu.edu.cn. Tel. & Fax: 86-28-85412798.

(1) Huang, Y.; Duan, X.; Wei, Q.; Lieber, C. M. *Science* **2001**, *291*, 630–633.
(2) Burda, C.; Chen, X.; Narayanan, R.; El-Sayed, M. A. *Chem. Rev.* **2005**, *105*, 1025–1102.
(3) Jun, Y.; Choi, J.; Cheon, J. *Angew. Chem., Int. Ed.* **2006**, *45*, 3414–3439.
(4) Liu, J.; Wang, X.; Peng, Q.; Li, Y. *Adv. Mater.* **2005**, *17*, 764–767.
(5) Potyrailo, R. A.; Mirsky, V. M. *Chem. Rev.* **2008**, *108*, 770–813.
(6) (a) Nakagawa, M.; Kawabata, S.; Nishiyama, K.; Utsunomiya, K.; Yamamoto, I.; Wada, T.; Yamashita, Y.; Yamashita, N. *Sens. Actuator, B* **1996**, *34*, 334–338. (b) Nakagawa, M.; Okabayashi, T.; Fujimoto, T.; Utsunomiya, K.; Yamamoto, I.; Wada, T.; Yamashita, Y.; Yamashita, N. *Sens. Actuator, B* **1998**, *51*, 159–162.
(7) (a) Zhu, Y.; Shi, J.; Zhang, Z.; Zhang, C.; Zhang, X. *Anal. Chem.* **2002**, *74*, 120–124. (b) Lv, Y.; Zhang, S.; Liu, G.; Huang, M.; Zhang, X. *Anal. Chem.* **2005**, *77*, 1518–1525. (c) Sun, Z.; Yuan, H.; Liu, Z.; Han, B.; Zhang, X. *Adv. Mater.* **2005**, *17*, 2993–2997.
(8) (a) Na, N.; Zhang, S.; Wang, S.; Zhang, X. *J. Am. Chem. Soc.* **2006**, *128*, 14420–14421. (b) Wang, X.; Na, N.; Zhang, S.; Wu, Y.; Zhang, X. *J. Am. Chem. Soc.* **2007**, *129*, 6062–6063.
(9) Yang, P.; Ye, X. N.; Lau, C.; Li, Z. X.; Liu, X.; Lu, J. Z. *Anal. Chem.* **2007**, *79*, 1425–1432.

 Published on Web 10/14/2009

industry for their porous structure, richer mixed-valence and p-type semiconducting properties and wide applications in catalyst, ion exchange, molecular adsorption, gas sensing, and energy storage in secondary batteries.[10] Although natural mineral manganese oxides are widely available, their activities and properties are not reproducible due to their nonuniform structures.[11] Therefore, different synthesis methods including ion-exchange, reflux, coprecipitation, sol−gel, solid-state chemical reaction,[12] template-assisted,[13] electrodeposition,[14] and hydrothermal treatment have been developed to produce uniform MnO_x nanostructures by several groups.[15−19] Hydrothermal synthesis is a powerful technique to prepare micro/nano materials with different architectures such as nanorods,[20] nanowires,[21] and nanotubes,[22] even more complex constructing hierarchical structures or networks.[23−25] Zhang et al. have controllably synthesized several polymorphic forms of manganese oxide, such as δ-MnO_2 nanosheets, γ-MnO_2 microspheres, β-MnO_2 distinct rods and semitubes, birnessite-related manganese oxide spindly nanowire bundles, and flower-like microspheres previously.[26] By proper choice of the temperature, time, and reactants for the hydrothermal process, the desired micro/nano architectures can be controllably synthesized.

Generally, each structure has its own characteristics which depends on various factors such as powder size, dimension, composition, crystalline structure, or bulk density.[27−29] Wang's group has demonstrated that the catalytic performance of nanocrystals can be finely tuned by their shape and composition.[30] Suib et al. has also pointed out that the reactivity of active manganese oxides depends on their preparation methods, compositions, and structures.[31] Because the specific nature of the material governs the selectivity of all catalytic reactions and the morphological/structural difference of the catalytic micro/nano materials leads to different CTL responses,[8] it is desirable but remains a challenge to controllably synthesize micro/nano materials with different morphologies to meet the analytical demand for improving sensitivity and selectivity to particular volatile organic compounds (VOCs).

In the present work, we controllably synthesized two novel shapes of Mn_3O_4 micro-octahedra and hexagonal nanoplates through a facile hydrothermal route. To the best of our knowledge, the novel shapes of Mn_3O_4 micro-octahedra and hexagonal nanoplates are first been controllably synthesized. We further designed new acetone sensors by equipping the prepared materials with cataluminescence properties. Sensing tests show that the CTL properties of synthesized Mn_3O_4 materials are shape-dependent and Mn_3O_4 micro-octahedra shows potential applications for acetone gas sensors.

Experimental Section

Chemical Reagents. All chemicals are of analytical-grade without further purification. $KMnO_4$, Na_2SO_3, H_2O_2, HCl, ethanol, and acetone are supplied by Chengdu Kelong Chemical Reagent Company (China), while *n*-dodecylamine ($C_{12}H_{27}N$) is from ABCR GmbH & Co. KG.

Sample Preparation. A typical synthesis procedure for Mn_3O_4 micro-octahedra was as follows: (1.85 g) *n*-dodecylamine and (3.78 g) Na_2SO_3 were dissolved in (38 mL) ethanol with vigorous stirring. When the solution clarified, (3.16 g) $KMnO_4$ was added with continuously stirring. The resultant solution was then transferred into a Teflon-lined stainless steel autoclave (50 mL) and maintained at 180 °C for 2 days. When the amount of *n*-dodecylamine was increased to (3.70 g) with hydrothermal time of one day but without Na_2SO_3, the Mn_3O_4 hexagonal nanoplates were obtained. The resulting brown products were collected by filtration, washed with deionized water, and then air-dried at 80 °C for the following characterizations. The morphology can be controllably tuned by adjusting hydrothermal treatment time and selecting reducing agents, and the formation mechanism for the Mn_3O_4 micro-otcahedra and hexagonal nanoplates are discussed in the Supporting Information (Figures S1 and S2).

Apparatus and Characterization. The powder X-ray diffraction patterns were recorded with a X'Pert Pro X-ray diffractometer with Cu Kα (λ = 1.5406 Å), using an operation voltage of 40 kV and a current of 40 mA, respectively. The morphology of the as-prepared Mn_3O_4 samples was examined using a JSM-5900LV scanning electron microscope operated at an accelerating voltage of 20 kV. A Quantachrome SI instrument was used to measure the surface area of obtained materials. Samples were predegassed at 300 °C for about 3 h to remove water and other

(10) Feng, Q.; Kanoh, H.; Ooi, K. *J. Mater. Chem.* **1999**, *9*, 319–333.
(11) Shen, X. F.; Ding, Y. S.; Hanson, J. C.; Aindow, M.; Suib, S. L. *J. Am. Chem. Soc.* **2006**, *128*, 4570–4571.
(12) Liu, Z. H.; Kang, L. P.; Zhao, M. Z.; Ooi, K. *J. Mater. Res.* **2007**, *22*, 2437–2447.
(13) Li, X. X.; Cheng, F. Y.; Guo, B.; Chen, J. *J. Phys. Chem. B* **2005**, *109*, 14017–14024.
(14) Li, Q. G.; Olson, J. B.; Penner, R. M. *Chem. Mater.* **2004**, *16*, 3402–3405.
(15) Subramanian, V.; Zhu, H.; Vajtai, R.; Ajayan, P. M.; Wei, B. *J. Phys. Chem. B* **2005**, *109*, 20207–20214.
(16) Li, Z.; Ding, Y.; Xiong, Y.; Xie, Y. *Cryst. Growth Des.* **2005**, *5*, 1953–1958.
(17) Yuan, J.; Li, W. N.; Gomez, S.; Suib, S. L. *J. Am. Chem. Soc.* **2005**, *127*, 14184–14185.
(18) Patrice, R.; Dupont, L.; Aldon, L.; Jumas, J. C.; Wang, E.; Tarascon, J. M. *Chem. Mater.* **2004**, *16*, 2772–2782.
(19) Wang, X.; Li, Y. *J. Am. Chem. Soc.* **2002**, *124*, 2880–2881.
(20) Liu, J.; Son, Y. C.; Cai, J.; Shen, X. F.; Suib, S. L.; Aindow, M. *Chem. Mater.* **2004**, *16*, 276–285.
(21) Yuan, Z. Y.; Zhang, Z. L.; Du, G. H.; Ren, T. Z.; Su, B. L. *Chem. Phys. Lett.* **2003**, *378*, 349–353.
(22) Zheng, D.; Sun, S.; Fan, W.; Yu, H.; Fan, C.; Cao, G.; Yin, Z.; Song, X. *J. Phys. Chem. B* **2005**, *109*, 16439–16443.
(23) Cheng, F.; Zhao, J.; Song, W.; Li, C.; Ma, H.; Chen, J.; Shen, P. *Inorg. Chem.* **2006**, *45*, 2038–2044.
(24) Wu, C.; Xie, Y.; Wang, D.; Yang, J.; Li, T. *J. Phys. Chem. B* **2003**, *107*, 13583–13587.
(25) Li, W.; Yuan, J.; Shen, X. F.; Gomez, M. S.; Xu, L. P.; Sithambaram, S.; Aindow, M.; Suib, S. L. *Adv. Funct. Mater.* **2006**, *16*, 1247–1253.
(26) (a) Zhang, L. C.; Liu, Z. H.; Lv, H.; Tang, X.; Ooi, K. *J. Phys. Chem. C* **2007**, *111*, 8418–8423. (b) Zhang, L. C.; Kang, L. P.; Lv, H.; Su, Z. H.; Ooi, K.; Liu, Z. H. *J. Mater. Res.* **2008**, *23*, 780–789.
(27) Wang, L. Z.; Ebina, Y.; Takada, K.; Sasaki, T. *Chem. Commun.* **2004**, *9*, 1074–1075.
(28) Sun, Y.; Xia, Y. *Science* **2002**, *298*, 2176–2179.
(29) Kan, S.; Mokari, T.; Rothenberg, E.; Banin, U. *Nat. Mater.* **2003**, *2*, 155–158.
(30) Tian, N.; Zhou, Z. Y.; Sun, S. G.; Ding, Y.; Wang, Z. L. *Science* **2007**, *316*, 732–735.
(31) (a) Son, Y. C.; Makwana, V. D.; Howell, A. R.; Suib, S. L. *Angew. Chem., Int. Ed.* **2001**, *40*, 4280–4283. (b) Tian, Z. R.; Tong, W.; Wang, J. Y.; Duan, N. G.; Krishnan, V. V.; Suib, S. L. *Science* **1997**, *276*, 926–930.

Scheme 1. Scheme of the CTL sensor Configuration

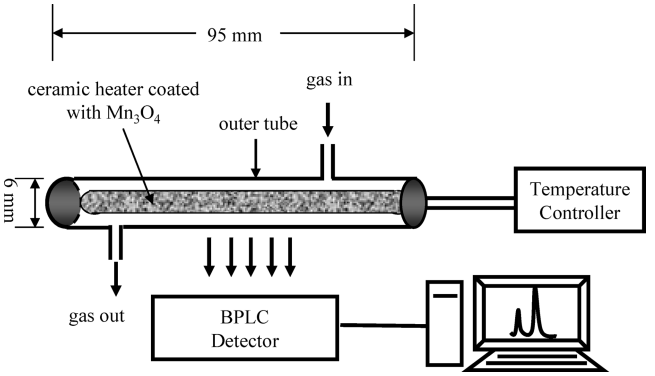

physically adsorbed species. The N_2 isothermal adsorption and desorption experiments were performed at relative pressures (P/P_0) from 0.05 to 0.99 and from 0.99 to 0.10, respectively. XPS spectra of the synthesized Mn_3O_4 micro-octahedra were obtained with an Axis Ultra, Kratos (UK) using monochromatic Al Ka radiation (150 W, 15 kV, and 1486.6 eV), and XPS of the synthesized hexagonal nanoplates using Mg as the exciting source. Binding energy was calibrated relative to the C 1s peak (284.8 eV) from hydrocarbons adsorbed on the surface of the samples. The magnified HRTEM images and corresponding selective area electron diffraction (SAED) were characterized by means of a high-resolution transmission electron microscope (HRTEM, Tecnai G^2 F20 S-Twin) at an accelerating voltage of 200 kV.

Sensor Configuration. As shown in Scheme 1, the CTL sensor system consists of two main parts: a homemade reaction cell coupled with a voltage controller and a commercial BPCL ultraweak luminescence analyzer (Biophysics Institute of Chinese Academy of Science, Beijing, China). About (0.035 g) prepared Mn_3O_4 micro-octahedra or hexagonal nanoplates were coated as a layer on a ceramic heating tube, respectively, which was put into a quartz tube (i.d. = 6 mm and length = 95 mm) to form the reaction cell. The air from the pump was mixed with acetone and flowed through the quartz tube, where acetone was oxidized on the surface of the catalyst by oxygen gas in the air and emitted light for detection.

Results and Discussion

Structure and Morphology. The XRD patterns of the prepared Mn_3O_4 micro-octahedra and hexagonal nanoplates are shown in Figure 1. The XRD pattern of Mn_3O_4 micro-octahedra (Figure 1a) can be closely indexed to pure tetragonal Mn_3O_4 (space group $I41/amd$ (No. 141)) with lattice parameters $a = b = 5.759$ Å and $c = 9.454$ Å. All strong peak positions and profiles are in good agreement with those reported in the literature for hausmannite Mn_3O_4 (JCPDS 24−0734). On the other hand, hexagonal nanoplates are composed of two phases of manganese oxides (Figure 1c), which are the Mn_3O_4 phase (JCPDS 24−0734) for the most part and a very small fraction peak at 2θ value of 19.19° assigned to cubic

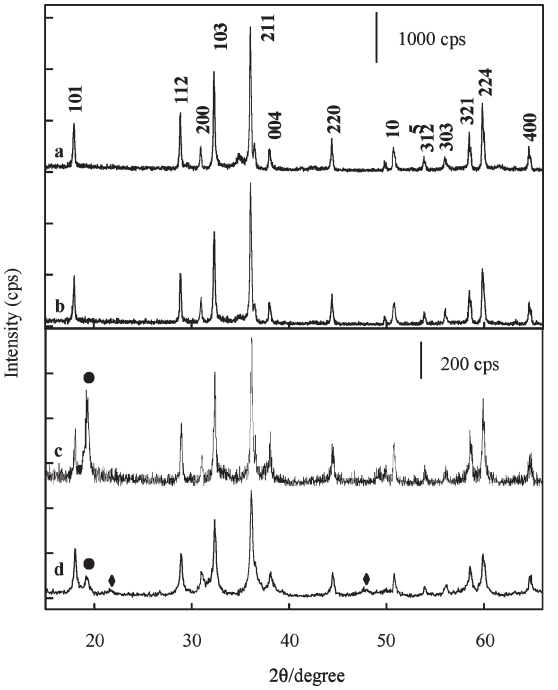

Figure 1. XRD patterns of the materials. (a, b) Mn_3O_4 micro-octahedra before and after the CTL test; and (c, d) hexagonal nanoplates before and after the CTL test. ●. MnO_2; ♦. Mn_5O_8.

MnO_2 phase (JCPDS 42−1169). The quantity and composition are obtained by chemical analysis, atomic absorption spectrometry, the average oxidation state ($Z_{Mn}{}^{a}$) of framework manganese,[32] and X-ray photoelectron spectroscopy (see the Supporting Information, Table S1 and Figure S3). Elemental analysis (Table S1) indicates that the prepared micro-octahedra has a chemical formula of $Mn_3O_{3.99}$ with an average oxidation state of manganese 2.65, which is almost the same as that of hausmannite-Mn_3O_4. The prepared hexagonal nanoplates have a chemical formula of $Mn_3O_{4.26}$ with the average oxidation state of manganese 2.84, including 87% Mn_3O_4 and 13% MnO_2, which is consistent with the mixed Mn_3O_4−MnO_2 manganese oxide system verified by the XRD pattern of Figure 1c. X-ray photoelectron spectra (Figure S3 in the Supporting Information) indicate that the Mn2p region consists of a spin−orbit doublet with binding energy of 653.6 eV ($Mn2p_{1/2}$) and 641.7 eV ($Mn2p_{3/2}$) for Mn_3O_4 micro-octahedra and 653.1 eV ($Mn2p_{1/2}$) and 641.4 eV ($Mn2p_{3/2}$) for hexagonal nanoplates, which are characteristic of a mixed-valence manganese system (Mn^{4+} and Mn^{2+}).[33]

SEM images display the size and morphologies of two prepared materials in Figure 2. They have the same Mn_3O_4 phase generally but exhibit completely different morphologies. The product obtained from dodecylamine-Na_2SO_3-ethanol solution shows unique octahedra morphology with arris ranging 1−3 μm (Figure 2a, b) and the other product obtained from dodecylamine-ethanol shows uniform hexagonal plate morphology with side

(32) (a) Manganese Ores-Determination of Manganese Content-Potentiometric Method and Ammonium Iron (II) Sulphate Titrimetric Method (GB/T 1506−2002, China). (b) *Methods for Determination of Active Oxygen in Manganese Ores; Japan Industrial Standard* (*JIS*); Japanese Standards Association: Tokyo, 1969; p M 8233.

(33) (a) Cao, H.; Suib, S. L. *J. Am. Chem. Soc.* **1994**, *116*, 5334–5342. (b) Tan, B. J.; Klabunde, K. J.; Sherwood, P. MA *J. Am. Chem. Soc.* **1991**, *113*, 855–861.

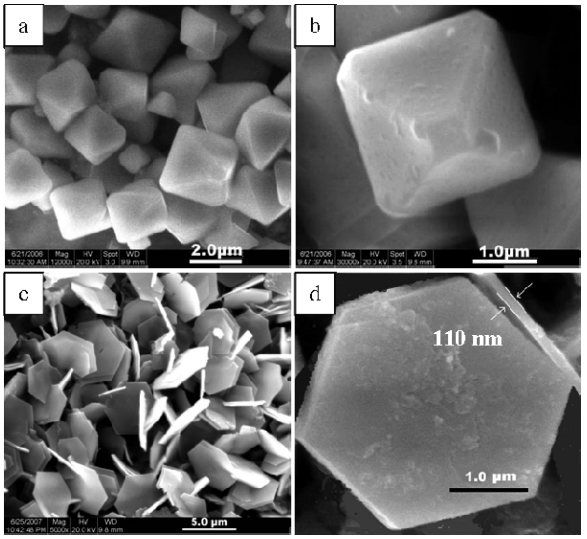

Figure 2. SEM images of prepared Mn_3O_4 micro-octahedra and hexagonal nanoplates: (a) Mn_3O_4 micro-octahedra; (b) a single Mn_3O_4 micro-octahedra with higher magnification; (c) hexagonal nanoplates; and (d) a single hexagonal nanoplate with higher magnification.

edge of ca. 2 μm and thickness of ca. 110 nm (Figure 2c, d). There were no other nonuniform particles found in both the panoramas of micro-octahedra and hexagonal nanoplates (Figure 2a, c). This suggests that the novel Mn_3O_4 micro-otcahedra and hexagonal nanoplates can be controllably synthesized by adjusting hydrothermal treatment time and selecting reducing agents.

Cataluminescence Property. On-site and real-time monitoring of acetone is necessary because acetone, an easily volatile chemical reagent, is frequently used to dissolve plastics, purify paraffin, and dehydrate tissues, and for pharmaceutical applications. People may develop a headache, fatigue, and even narcosis when the concentration of acetone is high in the air. Acetone levels in diabetic patients' blood and spittle are higher than those of healthy people.[34] There are many types of acetone sensor such as semiconductor sensors, amperometric-based sensors, luminescence-based sensors, piezoelectric sensors, and so on. Each type of sensor has its own advantages which originated from their sensing principles.[35] Sensors based on CTL show some significant advantages, such as high sensitivity, good selectivity and fast response. The good catalytic activity of manganese oxides makes MnO_x nanostructures likely to be good sensing materials, so the prepared manganese oxides are assembled to CTL sensors for trace acetone. Scheme 1 shows the CTL sensor configuration.

The CTL properties of the prepared manganese oxides were investigated by continual injection 130 μg mL^{-1} acetone vapor with an air flow rate at 500 mL min^{-1}. The Mn_3O_4 micro-octahedra and hexagonal nanoplates

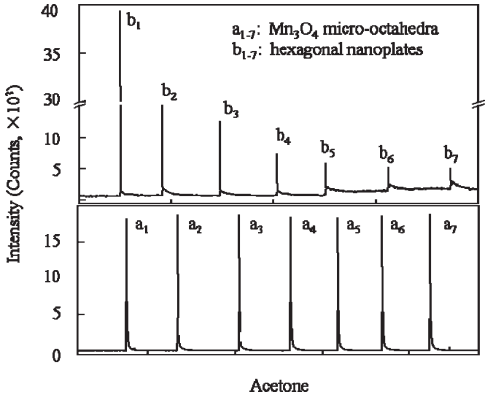

Figure 3. Typical CTL intensity of 131 μg mL^{-1} acetone vapor on the prepared Mn_3O_4 micro-octahedra and hexagonal nanoplates. Air flow rate, 500 mL min^{-1}; temperature, 284 °C.

exhibit different CTL response to acetone. As shown in Figure 3, a series of strong and steady CTL signals were obtained with the Mn_3O_4 micro-octahedra. Although higher signals were observed with the hexagonal nanoplates at early stage, they quickly decreased and finally disappeared. In order to investigate the reasons why the CTL responses are so different and why the CTL signals attenuated so rapidly, the XRD patterns and SEM images of Mn_3O_4 micro-octahedra and hexagonal nanoplates were taken before and after the CTL tests.

The XRD patterns of Mn_3O_4 micro-octahedra (Figure 1a, 1b) remain the same before and after the CTL test, and both can be closely indexed to pure tetragonal Mn_3O_4. On the other hand, the Mn_3O_4 hexagonal nanoplates were composed of two phases of manganese oxides (Figure 1c), including the Mn_3O_4 phase (JCPDS 24−0734) for the most part and a very small fraction of cubic MnO_2 phase (JCPDS 42−1169). After the CTL test, the MnO_2 phase in Mn_3O_4 hexagonal nanoplates sample gradually changed (Figure 1d) and the covered films apparently became black from brown. The diffraction peaks at 2θ values of 21.63 and 47.81° are assigned to the monoclinic phase of Mn_5O_8 (JCPDS 39−1218).

Before and after the CTL tests, there is no change in morphologies for Mn_3O_4 micro-octahedra (Figure 4a), whereas the morphologies of hexagonal nanoplates change significantly after use (Figure 4b, 4c). Hexagonal nanoplates were broken into pieces, to which many irregular particles adhered. Combining XRD data analysis (Figure 2c, 2d), the MnO_2 phase in the hexagonal nanoplates gradually reduced to Mn_5O_8 and Mn_3O_4 phases during the CTL procedure in the air flow at about 284 °C. The neonatal Mn_5O_8 and Mn_3O_4 phases covered and eliminated the active sites of the manganese oxide, so the material gradually lost the catalytic activity toward acetone. These results show that both materials phase and morphology are important influencing factors on sensor performance.

In general, the catalytic activity of materials is connected with their surface areas. Mn_3O_4 micro-octahedra have higher Brunauer−Emmett−Teller (BET) surface area (46 m^2/g) than that of hexagonal nanoplates

(34) Wang, C. C.; Weng, Y. C.; Chou, T. C. *Sens. Actuators, B* **2007**, *122*, 591–595.
(35) (a) Anno, Y.; Maekawa, T.; Tamaki, J.; Asano, Y.; Hayashi, K. *Sens. Actuator, B* **1995**, *24*, 623–627. (b) Makisimovich, N.; Vorotyntsev, V.; Nikitina, N.; Kaskevich, O.; Karabun, P.; Martynenko, F. *Sens. Actuator, B* **1996**, *6*, 419–421. (c) Bark′o, G.; Hlavay, J. *Anal. Chim. Acta* **1998**, *367*, 135–143.

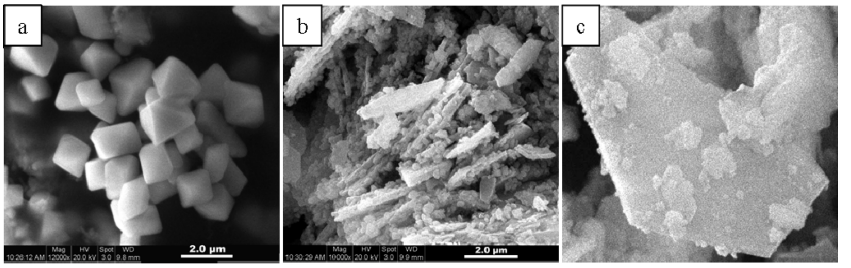

Figure 4. SEM images of materials after the CTL tests: (a) Mn_3O_4 micro-octahedra, (b) hexagonal nanoplates, and (c) a higher magnification of hexagonal nanoplate.

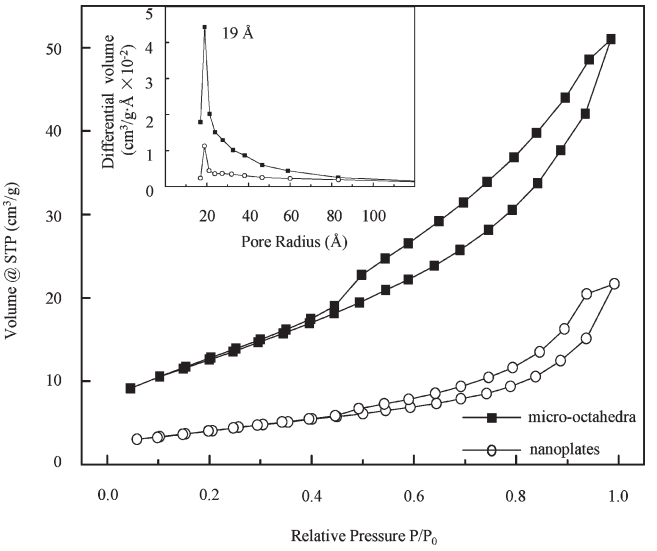

Figure 5. N_2 physisorption isotherms with the pore size distribution by the BJH method (inset): (a) Mn_3O_4 micro-octahedra and (b) hexagonal nanoplates.

($15\ m^2/g$). The isotherms showed that both Mn_3O_4 micro-octahedra and hexagonal nanoplates had a BDDT type IV with hysteresis loop which is characteristic of mesoporous materials (Figure 5 and inset). However, compared to those typical mesoporous materials, the fraction of mesopores is not so large according to the calculated results by the Barrett−Joyner−Halenda (BJH) method. The pore size distributions affected by morphologies and structures of materials may be related with the distribution of the active sites. At the same time, the Miller-index of the crystal plays an important role in the catalytic activity and stability. Li's group showed that the different reactivity and selectivity of catalysts depend greatly upon the different arrangement manner of surface atoms, depending on their Miller indices. In fact, the exposed crystal planes (Miller indices) are determined by the morphologies and phases of nanocrystals.[36] As can be seen from the magnified HRTEM images and corresponding selective area electron diffraction (SAED) from a typical Mn_3O_4 micro-octahedron and nanoplate (Figure 6a and 6b), the dominant exposed planes of Mn_3O_4 micro-octahedra are {351}, which are the planes normal to both the set of (103) planes with a lattice space of 0.28 nm and the set of (112) planes with a lattice space

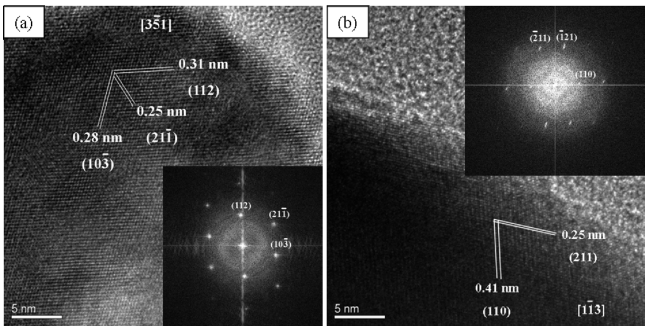

Figure 6. HRTEM images and corresponding selective area electron diffraction (SAED) from a typical Mn_3O_4 micro-octahedron and a nanoplate: (a) micro-octahedra and (b) nanosheets.

of 0.31 nm while the dominant exposed plane of hexagonal nanosheets are {113}. These results are in agreement with those reported in the literature. Wang's group has pointed out those high-index planes of single-crystal surfaces generally exhibit much higher catalytic activity than that of the most common stable planes.[37] However, because of the multidimensional nature of the interactions between the function and the end-use conditions of materials, the exploration to the truth what determines the catalytic activity is still a great challenge. We observed the CL emission and tried to further clarify its generation mechanism of the oxidation reaction in a recent work.[38] With attention paid to sensing material and understanding the interactions between gas molecules and materials, further studies are under way in our group.

We chose Mn_3O_4 micro-octahedra as a sensing material to further study the analytical characteristics of the CTL sensor for acetone. Under the optimal experimental conditions (see the Supporting Information, Figures S4−S6), the present sensor has a fast response time of 3 s and recovery time of less than 40 s, with a limit of detection (LOD) of $0.4\ \mu g\ mL^{-1}$ (signal/noise = 3). Meanwhile, the present sensor has a high selectivity toward acetone. It can be seen from Figure S7 in the Supporting Information that 11 common VOCs tested under the same conditions, including methanol, ethanol, propanol, benzene, cyclohexane, ethylacetate, formaldehyde, acetaldehyde, dichloromethane, chloroform, and carbon tetrachloride at concentrations ranging from 5 to

(36) Hu, L.; Peng, Q.; Li, Y. *J. Am. Chem. Soc.* **2008**, *130*, 16136–16137.
(37) Tian, N.; Zhou, Z.; Sun, S.; Ding, Y.; Wang, Z. *Science* **2007**, *316*, 732–735.
(38) Hu, J.; Xu, K.; Jia, Y.; Lv, Y.; Li, Y.; Hou, X. *Anal. Chem.* **2008**, *80*, 7964–7969.

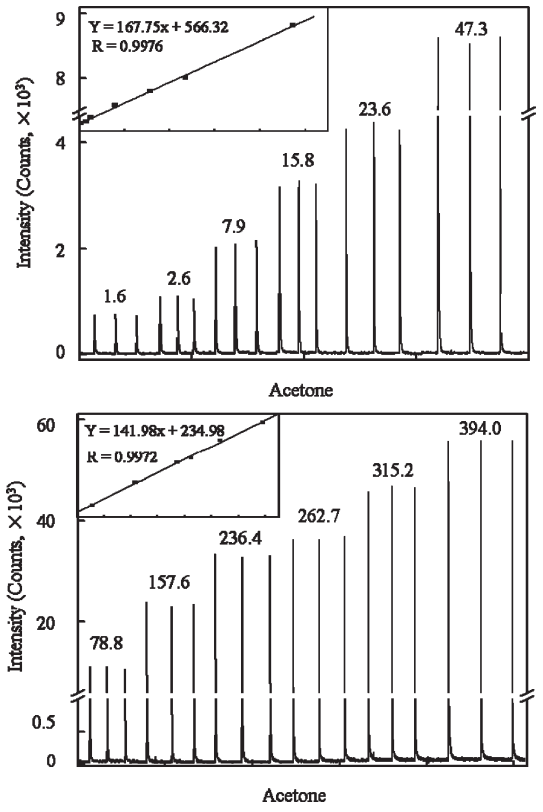

Figure 7. Typical relative CTL intensity versus acetone vapor concentration (μg mL^{-1}). Air flow rate, 500 mL min^{-1}; temperature, 284 °C. For the linear regression equations, r is the correlation coefficient, Y is the CTL intensity, and X is the concentration of acetone vapor.

500 μg mL^{-1}, does not significantly interfere with acetone CTL response because the largest signal variation (for propanol) is equivalent to the largest standard deviation of the measurements. However, when acetone-propanol or acetone-acetaldehyde mixture (1 + 1) was used for the test, acetone signal can be depressed by 18−22%. This means standard addition method is still needed for calibration or a preseparation step is necessary, when propanol or acetaldehyde content is high in real sample analysis. It also gives a high tolerance to water vapor. As shown in Figure S8 in the Supporting Information, it is obvious that the catalytic activity of sensing material is not affected by water vapor at 284 °C. Figure 7 shows the signal intensities and reproducibility from a series of acetone concentrations. As shown in Figure 7 (inset), the calibration curve of the CTL intensity versus acetone vapor concentration was linear in two ranges of 2.6−52.2 μg mL^{-1} and 52.2−394.0 μg mL^{-1}, respectively. Each point in Figure 7 is the average of three replicates, of which the relative standard deviation (RSD) is in the range of 1 to 3%. In terms of long-term stability, the signal variation of acetone concentration at 47 μg mL^{-1} varied within ±11% in 6 months.

Conclusions

Mn_3O_4 micro-octahedra and hexagonal nanoplates can be controllably synthesized simply by a facile hydrothermal process, and the former shows better CTL sensing characteristic to acetone gas. The acetone gas sensor using Mn_3O_4 micro-octahedra shows several advantages: (a) high detectability with an LOD as low as 0.4 μg mL^{-1}; (b) good selectivity that nine common volatile organic compounds would not significantly interfere with the determination of acetone vapor; and (c) good short-term and long-term stability, less than 3% RSD and ±11% variation, respectively. The different morphological and structural Mn_3O_4 materials present different CTL properties toward acetone, which not only provides some interesting information to the synthesis of materials but also offers some kinetic performance in adsorption and catalysis areas. Further, the fact of shape-dependent cataluminescence demonstrates that controllable synthesis of materials is an effective way to improve the sensor performance.

Acknowledgment. The authors gratefully acknowledge the National Nature Science Foundation of China (20835003) and Ministry of Science and Technology of China (2007AA03Z248 and 2007CB936102) for financial support. We also thank Dr. Ming Liu and Mr. Xuejiang Wang of Analytical & Testing Center at Sichuan University for assistance with the HRTEM and chemical analysis.

Supporting Information Available: Chemical composition, crystal growth mechanism, XPS, optimal sensing conditions, CTL spectra of response/recovery time, sensor selectivity, and interference of water (PDF). This material is available free of charge via the Internet at http://pubs.acs.org.